J Mater Sci (2011) 46:400–408
DOI 10.1007/s10853-010-4853-1

Influence of hybrid organic–inorganic sol–gel matrices on the photophysics of amino-functionalized UV-sensitizers

M. Oubaha · R. Copperwhite · C. Boothman · A. Ovsianikov · R. Kiyan · V. Purlys · M. O'Sullivan · C. McDonagh · B. Chichkov · R. Gadonas · B. D. MacCraith

Received: 6 April 2010 / Accepted: 19 August 2010 / Published online: 3 September 2010

Abstract Recent interest in photolithographic processes employing single and two-photon absorption processes have afforded advanced opportunities to fabricate both planar and three-dimensional microstructures. The fabrication of such structures is dependent on the local polymerization of the organic moieties using photoinitiating molecules, and a key parameter to consider is the dependency of the photoreactivity of these initiators on the matrices in which they are dispersed. To our knowledge, there has been no comprehensive investigation reported on the photoreactivity dependency of commercially available photoinitiators inserted within hybrid sol–gel materials. The aim of this paper is to highlight and explain the influence of the composition of hybrid organic–inorganic sol–gel materials on the photoreactivity of UV-sensitive initiators. Of particular interest is the understanding of the interactions between photoinitiating molecules and the sol–gel matrix. It is shown that both the nature of the chelating agent as well as the degree of chelation of the inorganic part of the hybrid sol–gel material significantly influence the spectral absorption of the photoinitiator. It is demonstrated that metal–ligand charge transfer processes are the main phenomena responsible for the red shift of the absorption of the amino-functionalized photoinitiators, which is strongly dependent on the condensation of the materials.

M. Oubaha (✉) · R. Copperwhite · C. Boothman · M. O'Sullivan · C. McDonagh · B. D. MacCraith
National Centre for Sensor Research/Biomedical Diagnostics Institute, Dublin City University, Glasnevin, Dublin 9, Ireland
e-mail: Mohamed.Oubaha@dcu.ie

A. Ovsianikov · R. Kiyan · B. Chichkov
Nanotechnology Department, Laser Zentrum Hannover e.V, 30419 Hannover, Germany

V. Purlys · R. Gadonas
Department of Quantum Electronics, Vilnius University, Sauletekio 9, 10222 Vilnius, Lithuania

Introduction

Photocurable materials have attracted great interest over the past decade for micro/nanofabrication processes of two- and three-dimensional (3D) microstructures employing techniques such as UV-lithography [1–3] and two-photon polymerization (2PP) [4, 5]. The applications of such microstructures are constantly expanding and to date they have found use in fields as diverse as biotechnology [6], nanomedicine [7], information technology (e.g. micro/nanofluidic, biochips, photonic crystals, etc.) [8–11].

Fabrication of 2D microstructures is generally performed using the single-photon polymerization technique, which utilizes the linear optical absorption of UV-sensitive photoinitiators to cause the photoinduced crosslinking of organic molecules [12]. The fabrication of 3D microstructures has become possible with the recent development of the 2PP technique [2, 4, 13, 14], which exploits the multiphoton absorption of materials that are primarily UV-sensitive. The beam of an ultrafast laser, usually a femtosecond laser, operating in the visible or near infrared region, is tightly focused into the volume of a UV-photoreactive material. By moving the laser three-dimensionally through the material, any desired 3D structure can be fabricated. In theory, any photoreactive material (epoxy or acryloxy) in combination with a suitable photoinitiator (PI) can be employed either for the single photon or the 2PP technique. However, our recent investigations have

highlighted that compared to conventional organic resins, organic–inorganic hybrid sol–gel materials exhibit improved performance in terms of the resolution and shrinkage of the fabricated microstructures [15, 16]. Furthermore, interactions at the molecular level between the PIs and the sol–gel matrices may occur in certain conditions and strongly affect the global properties of the photosensitive material. To our knowledge, no study has focused on identifying the physico-chemical interactions between PIs and sol–gel matrices. This understanding is particularly important for the 2PP process, where non-linear processes are fundamental and must not overlap with the linear absorption of the material.

The aim of this article is to address this gap in understanding, by concentrating on the interactions between a well-established silicato-zirconate co-hybrid material [17] and three commercially available PIs (Irgacure 184 (I-184), Irgacure 369 (I-369) and 4,4′-diethylaminobenzophenone/Milcher's Ketone (DB)) that have recently shown high potential for employment in UV-lithography [18] and 2PP [15]. These PIs were selected for this study due to their different chemical structures, sterical properties and functional groups. Interactions at the molecular level have been identified employing UV–Visible spectroscopy and a proposed explanation of the observed results is based on the occurrence of the metal–ligand charge transfer processes (MLCT) between the PIs and the inorganic constituents of the developed hybrid materials.

Synthesis and characterization

Material development

The synthesis of the sol–gel matrix was based on the formation of a stable and homogeneous sol obtained from the mixture of a photosensitive organically modified silicate, the hybrid precursor 3-methacryloxypropyltrimethoxysilane (MAPTMS, $C_{10}H_{20}O_5Si$, Assay 99% in methanol, Aldrich), zirconium (IV) *n*-propoxide (ZPO, $C_{12}H_{28}O_4Zr$, Assay 70% in propanol, Aldrich), and a chelating agent, which is necessary to stabilize the zirconium (Zr) precursor in the presence of strong nucleophilic groups such as water. In a previous study [15], methacrylic acid (MAA, $C_4H_6O_2$, Assay >98%, Aldrich) was used as the chelating agent of ZPO (mixed with MAPTMS and ZPO in a molar ratio of 10:4.0:4.0, respectively). In this study we have altered the molar ratio of the precursors in order to assess the influence on the UV–visible absorption of the PIs. To this end we have changed the relative proportions of ZPO and MAA whilst keeping the amount of MAPTMS constant. The two new ratios are: 10:4.0:2.0 (formulation B) and 10:4.0:8.0 (formulation C). With the emphasis still on the chelating agent, in this study we have included an additional chelating agent, 2,2′-byripydil (BP, $C_{10}H_8N_2$, Assay 99%, Aldrich) for comparison with MAA. As summarized in Table 1, the molar ratios of this sol (formulation D) have been chosen to mirror formulation A.

Table 1 Summary of the material formulations

Formulation	Chelating agent	Molar ratio of the precursors MAPTMS:ZPO:chelating agent
A	MAA	10:4:4
B	MAA	10:4:2
C	MAA	10:4:8
D	BP	10:4:4

Due to the difference in reactivity of each of the alkoxide precursors present in the sols, the synthesis demands a three-step process: (1) pre-hydrolysis of the MAPTMS and complexation of ZPO with a chelating agent, (2) addition of the pre-hydrolysed organoalkoxysilane to the zirconate complex and (3) hydrolysis of the mixture. MAPTMS is hydrolysed employing an aqueous HCl 0.1 N solution in a 1.00:0.75 ratio. As MAPTMS and water are not miscible, the hydrolysis is initially performed in a heterogeneous way. The progressive production of methanol issued from the hydrolysis of MATPMS allows the miscibility of all species present in solution after 20 min of reaction. In parallel, the ZPO precursor was chelated by either MAA or BP, in order to reduce its reactivity with water, thus avoiding precipitation. After 45 min of reaction, the partially hydrolysed MAPTMS was slowly added to the zirconate complex. Following, 5 min of reaction, water (pH 7) was added dropwise to the mixture to complete the hydrolysis to 50% of the total alkoxide groups. A more detailed account of the sol–gel synthesis can be found in a previous article by the authors [16]. The concentration of the PIs was fixed at 1 mol% in all investigated formulations.

Two-photon polymerization technique

Two-photon polymerization is a direct laser writing technique, which allows the fabrication of complex 3D structures with a resolution below 100 nm [3, 4, 13, 19, 20]. In this study, a Ti:sapphire laser (Chameleon, Coherent) was used, delivering pulses of 140 fs duration at a repetition rate of 80 MHz and a central emission wavelength of 780 nm. A microscope objective lens (100×, NA = 1.4, Zeiss magnification) was used to focus the laser beam into the volume of the photosensitive material. The materials are transparent at the emission wavelength of the laser; therefore, only two-photon absorption associated with non-linear properties of the material can initiate a

photopolymerization reaction. Due to the threshold behaviour and nonlinear nature of the 2PP process, the light-material interaction region is confined to the small volume within the focus of the laser beam. Resolution beyond the diffraction limit can be realized by controlling the laser pulse energy and the number of applied pulses. In this step, the final organic–inorganic network is formed by polymerizing the pendant methacryloxy moieties. The material is polymerized along the trace of the moving laser focus, thus enabling fabrication of any desired polymeric 3D pattern by direct "recording" into the volume of a photosensitive material. In a subsequent processing step, the areas of the material that were not exposed to the laser radiation are removed by etching in 2-propanol, revealing the microfabricated structure.

Characterization techniques

The UV–visible absorption spectra (200–800 nm) were recorded using a Cary Varian 50 scan spectrophotometer with a resolution of 4 cm^{-1}. The scan speed was 600 nm/min. Liquid samples were prepared by sandwiching the liquid sol between two quartz films in order to obtain a film of 100 μm thickness. Measurements of solid samples were recorded using thin films deposited by spin-coating the different sol–gel solutions onto quartz slides and thermally stabilized at 100 °C for 2 h.

Results and discussion

Photophysical properties of the photoinitiators

Interaction within a zirconium-based sol–gel material

The UV–Visible absorption of the three pure PIs employed in this study are shown in Fig. 1. In the 200–500 nm range, I-184, I-369 and DB all exhibit one large absorption band centred at 240, 325 and 365 nm, respectively, which are assigned to the various π–π^* transitions of the aromatic groups contained in each molecule (Fig. 2).

The absorption in the liquid phase of the different PIs within material A is shown in Fig. 3. It is easily observable that the absorption of the I-184 is unchanged, having a similar absorption around $\lambda_{max} \cong 240$ nm. However, the materials composed of I-369 and DB both show a shift of the initial absorption observed in the pure PIs (Fig. 1) towards the higher wavelengths to $\lambda_{max} \cong 356$ nm and $\lambda_{max} \cong 375$ nm, respectively. Moreover, the spectrum of the material containing DB shows the appearance of a second band centred at $\lambda_{max} \cong 459$ nm, the area of which, calculated by the spectral decomposition using Gaussian equations, corresponds approximately to 32% of the band centred at $\lambda_{max} \cong 375$ nm. These observations suggest that the sol–gel matrix is not only acting as a dispersing system for the PIs, but interactions at the molecular level between PIs and the host matrices are occurring and

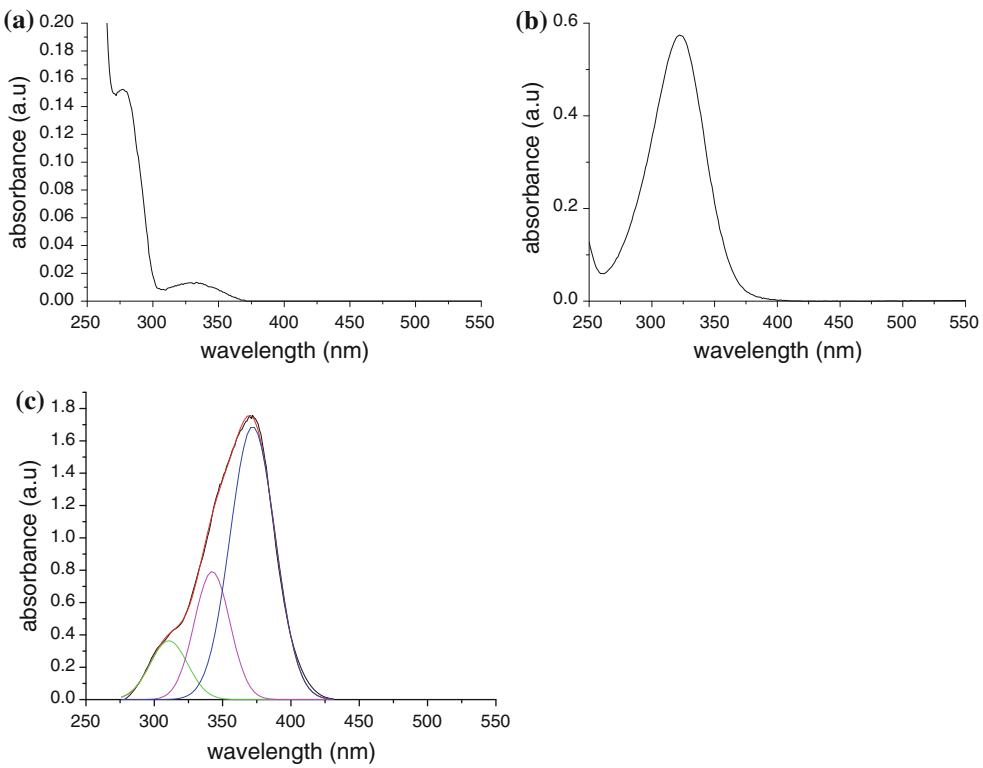

Fig. 1 UV–Visible spectra of **a** I-184, **b** I-369 and **c** DB, dissolved in isopropyl alcohol

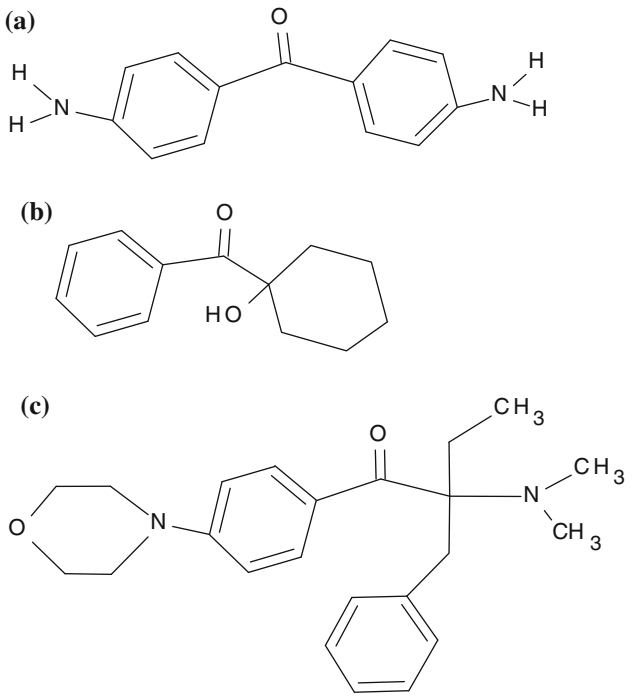

Fig. 2 Chemical structure of the photoinitiators used **a** 4,4′-diethylaminobenzophenone, **b** Irgacure 184 and **c** Irgacure 369

actively modifying the local environment of the PI molecules, resulting in strong modification of their spectral absorption. Comparison of the molecular structure of the three different PIs indicates that they all contain carboxy and aromatic groups, which cannot be considered as the only active groups because the maximum absorption peak of I-184 is not altered by the presence of the sol–gel matrix. However, in addition to these chemical groups, I-369 and DB both possess amino functions on their extremities (methylamine and ethylamine) that can potentially act as ligands in the presence of metal transition atoms. This is possible by the formation of coordinating bonds between the free pair of electrons located on the nitrogen atom and the d free-orbitals of the metal, in a similar way to the formation of metal–ligand complexes [21]. The physical consequence of this chemical reaction is known as the "Metal Ligand Charge Transfer" (MLCT) process [22], in which the electronic transition from the dπ (Zr) to the π* (PI) orbitals is facilitated by electron transfer from the transition metal towards the ligand. This process can support the absence of matrix effects on the I-184 and the red shift of the initial bands of the pure DB and I-369, but does not explain the appearance of the band around 459 nm in the case of DB only. This behaviour has been attributed to the difference in the structure of the PIs. In comparison with I-369, the structure of DB contains two nitrogen atoms that are potentially capable of acting as ligand to the Zr atom. The slight red shift of the initial band from

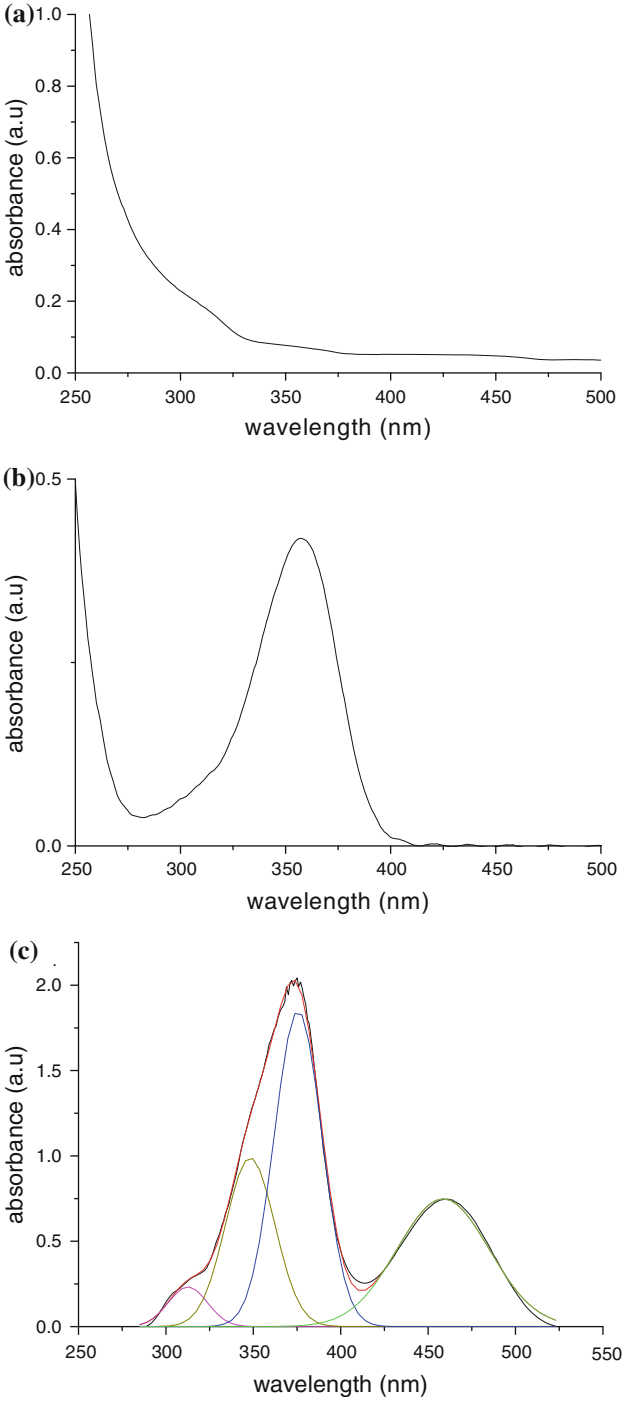

Fig. 3 UV–Visible spectra of **a** I-184, **b** I-369 and **c** DB dissolved in material A (liquid state samples)

$\lambda_{max} \cong 365$ nm to $\lambda_{max} \cong 375$ nm is not compatible with the appearance of a second band around $\lambda_{max} \cong 470$ nm, and signifies that both aromatic groups do not undergo the same matrix effect. To explain this behaviour, we propose that DB is only bonded to the SG matrix through one nitrogen atom, as sketched in Fig. 4. Within material A, the Zr atom is already partially chelated by the methacrylic

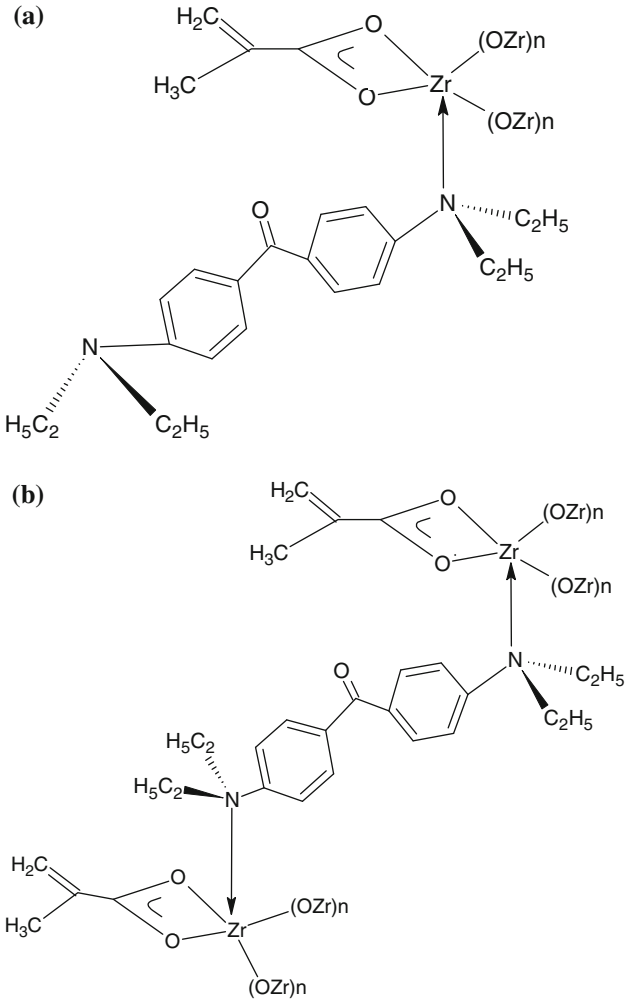

Fig. 4 Chemical structure of the DB within material A in the liquid **a** and solid **b** phases

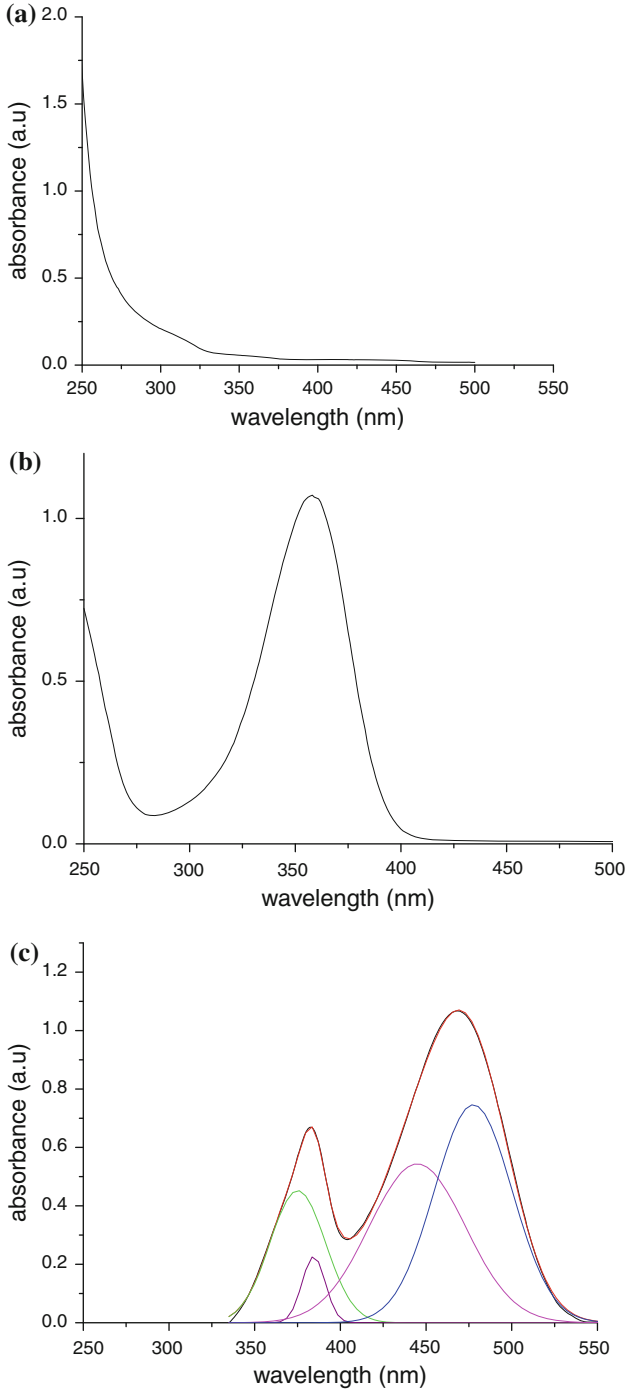

Fig. 5 UV–Visible spectra of **a** I-184, **b** I-369 and **c** DB dissolved in material A (solid state samples)

acid [17], and therefore, it is proposed that in the liquid phase the main reason limiting the entire linking of DB to the Zr atom is due to steric hindrance limitations. This hypothesis has motivated the investigation of the effect of the sol–gel condensation on the structure of the PIs, by recording UV–visible spectra of the developed materials in the solid state (thin films on quartz).

In the solid state, UV–Visible absorption spectra (Fig. 5) show that the absorption of both I-184 and I-369 remains at the same wavelength as in the liquid phase. However, for DB, both absorption bands undergo the same red shift of around 9 nm (from 372 to 381 nm and from 459 to 468 nm). Furthermore, unlike the liquid spectrum, the contribution of the bands located above 425 nm increases by 42% to reach 75% of the total band area, as quantified by the spectral decomposition. The mechanism of the solidification process involves the removal of the various alcoholic solvents, either present in the precursors employed or formed during the hydrolysis and condensation reactions inherent to the sol–gel synthesis. Solvent removal results in an increased connectivity of the inorganic network and entrapment of the PI in between the hybrid oligomers. The direct consequence is to diminish the steric hindrance restrictions and favour the formation of coordinating bonds between the PI and the transition metal, which were impossible in the liquid phase state. These

observations reinforce the hypothesis that the proximity factor is a critical point for the formation of the metal–ligand chemical bonds that favour the MLCT process. In the next section it will be shown that the material condensation has an influence on the photophysics of the PI, which can be evaluated by quantifying the effect of ZPO concentration along with the nature and concentration of the chelating agent employed.

Effect of the ZPO concentration on the PI absorption

In the previous section, it was highlighted that absorptions bands located above 400 nm are ascribable to the formation of chemical bonds between DB and the transition metal. Hence, the ratio of the bands area observed above and below 400 nm (named $R_1 = (\text{bands}_{(\lambda_{max} > 400)}/\text{all bands area})$ can be reasonably used to quantify the binding ratio between DB and the Zr atom. Furthermore, the ratio of the 2 bands areas located above 400 nm (named $R_2 = \lambda_{max(\sim 444)}/\lambda_{max(\sim 474)}$) band can be used to quantify the nature of the chemical bonds.

The UV–visible absorption spectra of materials containing an increasing ZPO/MAPTMS molar ratio and 1 mol% of DB are shown in Fig. 6. Compared to the spectra of pure DB (Fig. 1c) and the Zr-free material (Fig. 6a), one can observe that the introduction of 1% ZPO provokes the appearance of an extra band centred at 410 nm, resulting in a residual absorption until 500 nm, as demonstrated by the spectral decomposition (Fig. 6a).

A further increase of the ZPO content to 5% allows the extension of the absorption until 550 nm and a notable increase of R_1; which, however, saturates at around 72% for materials containing 10% or more of ZPO (Fig. 7).

Above 10 mol% of ZPO, one can also note that the different bands are located at the same position indicating that the essential structural modifications have occurred in the transition from materials containing up to 10% ZPO. However, R_2 increases progressively to reach 98% for the material containing the highest ZPO content (Fig. 7). From a structural point of view, this signifies that 98% of the DB molecules are linked to the Zr atom through two nitrogen atoms from the material containing 10% ZPO.

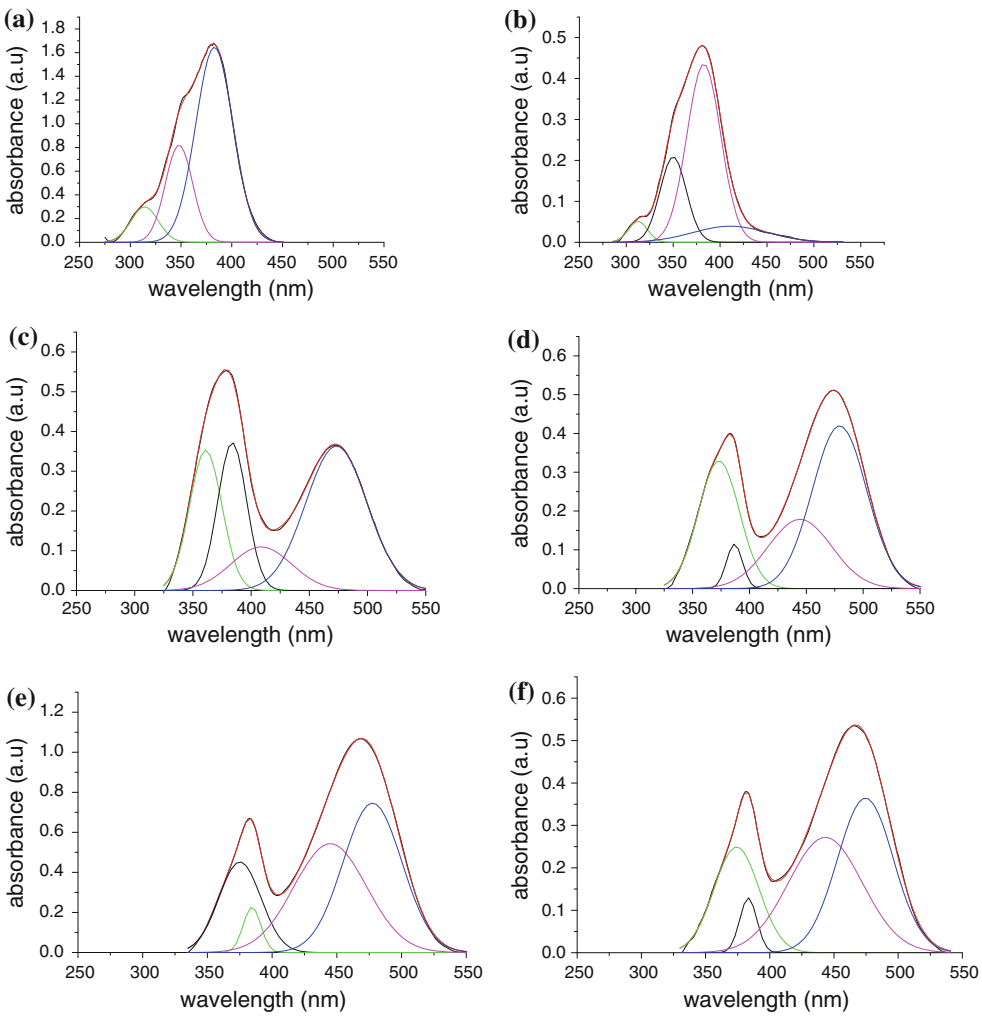

Fig. 6 UV–Visible spectra recorded on solid films of 1 mol% DB within materials containing 0 (**a**), 1 (**b**), 5 (**c**), 10 (**d**), 20 (**e**) and 30 mol% ZPO (**f**)

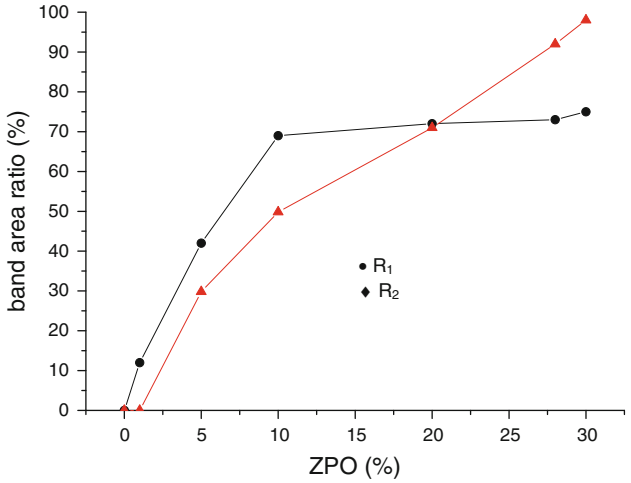

Fig. 7 Evolution of the bands area ratios $R_1 = (\text{bands}_{(\lambda_{max} > 400)}/$ all bands area) and $R_2 = \lambda_{max(\sim 444)}/\lambda_{max(\sim 474)}$ against the ZPO concentration

Effect of the chelating agent

In order to assess the effect of the steric hindrance around the Zr atom on its binding with DB, we have altered both the degree of chelation of the Zr atom and the nature of the chelating agent.

UV–Visible spectra of DB within materials B and C are shown in Fig. 8, in which the amount of MAA was adjusted to chelate 25 and 100% of the alkoxides groups contained in ZPO, respectively. As summarized in Table 2, the ratio between the band areas representing the binding of DB through 1 nitrogen atom (named band-1, located between 410 and 440 nm) and 2 nitrogen atoms (named band-2, located around 470 nm) decreases dramatically from 79.1 to 37.5% when the degree of chelation of the Zr atom increases. To account for the observed shift in the ratio of the two bands, it is proposed that a decrease of the chelation degree reduces the steric hindrance around the Zr atom allowing better accessibility to the ligand, which permits it to bind with the transition metal.

Table 2 Band-1/band-2 ratios for materials B and C

Materials	Ratio (%): band-1/band-2
B	79.1
C	37.5

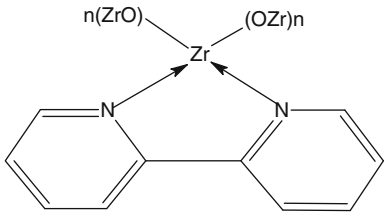

Fig. 9 Chemical structure of the ZPO chelated with BP

A further investigation of the nature of the chelating agent has been carried out by replacing MAA with 2,2′-bipyridyl (BP) (named material D). Unlike acid ligands, BP can form coordinating bonds with the zirconate complex (C–O–Zr), via the d free orbitals of the transition metals, as sketched in Fig. 9. The UV–Visible spectrum of material D containing 1% mol of DB (Fig. 10) does not exhibit any absorption band above 400 nm, the presence of which was established as an indication of a coordinating complex between a PI and ZPO (see 'Photophysical properties of the photoinitiators'). The absence of any such absorption in this case has been attributed to the prevention of any interaction between the PI and the Zr atom by steric hindrance.

It is concluded from the above results that the nature of the chelating agent as well as the degree of chelation can strongly modify the spectroscopic properties of the PI. The promotion or prevention of interactions between the transition metal and the PIs can be used as a tool to tune the spectral absorption of amino-functionalized PIs allowing precise adjustment of the photosensitive properties of these materials.

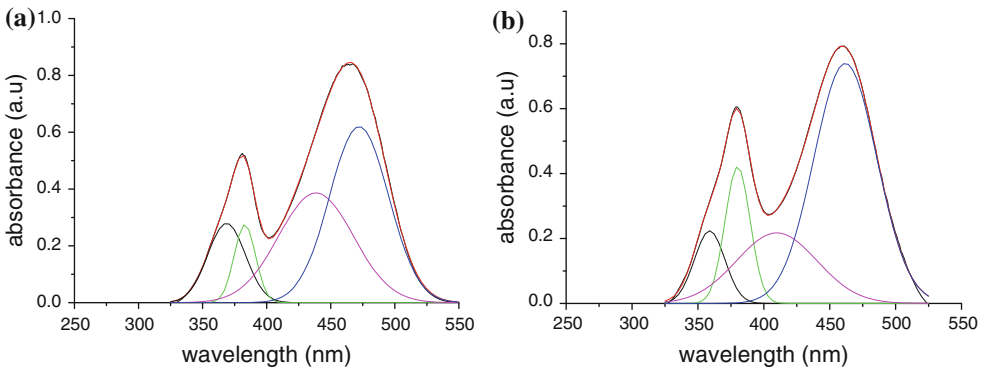

Fig. 8 UV–Visible spectra DB dissolved within materials B (**a**) and C (**b**) (solid state samples)

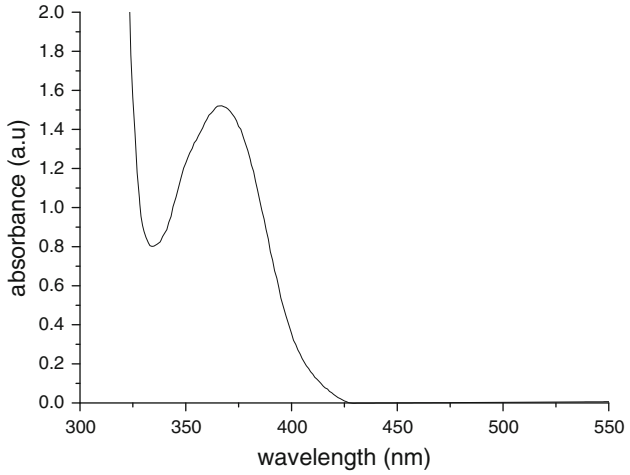

Fig. 10 UV–Visible spectrum of DB dissolved in material D (solid state samples)

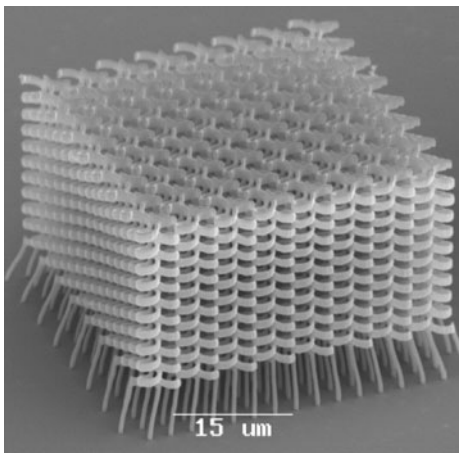

Fig. 12 Spiral three-dimensional photonic crystal

Influence of the ZPO content on the capability of 2PP microfabrication

The influence of the ZPO concentration on the dimensions of freely suspended lines (Fig. 11a) fabricated by the 2PP technique has been investigated. The lines are produced by a single scan at a constant velocity from the top of one supporting wall to the other. By applying higher laser powers larger line cross-sections (e.g. wider and higher voxels) are produced. The voxel height dependency on the ZPO concentration for four different laser powers (14, 25, 30 and 50 mW) is shown in Fig. 11b. At all presented laser powers it is possible to distinguish two characteristic curve regions depending on the material composition. From 0 to 10% of ZPO, the voxel sizes exhibit a logarithmic increase. Compared to the ZPO-free material, the addition of 1% of ZPO induces an average increase of 70% in the voxel size. Above 10% of ZPO, the voxel size increase relative to ZPO content is linear and much less pronounced with an average increase in voxel height of just 8%. As the laser power approaches 30 mW and higher, it is notable that only a 2% increase in voxel height is observed indicating a saturation behaviour. Nevertheless, in all cases, it was possible to fabricate non-shrinking three-dimensional structures, such as photonic crystals (Fig. 12).

These observations suggest that the material photoreactivity is strongly dependent on the ZPO concentration for materials containing up to 10% of ZPO. The comparative study conducted in 'Interaction within a zirconium-based sol-gel material' on the effect of the ZPO content on the DB absorption revealed that the absorption at 390 nm was progressively decreasing with the increase of ZPO, which is in contradiction with the behaviour observed in the present section. This clearly illustrates that the multiphoton absorption employed in the 2PP process cannot be directly correlated to the linear absorption of the materials. Investigations on the 2PP absorption are required to explain the

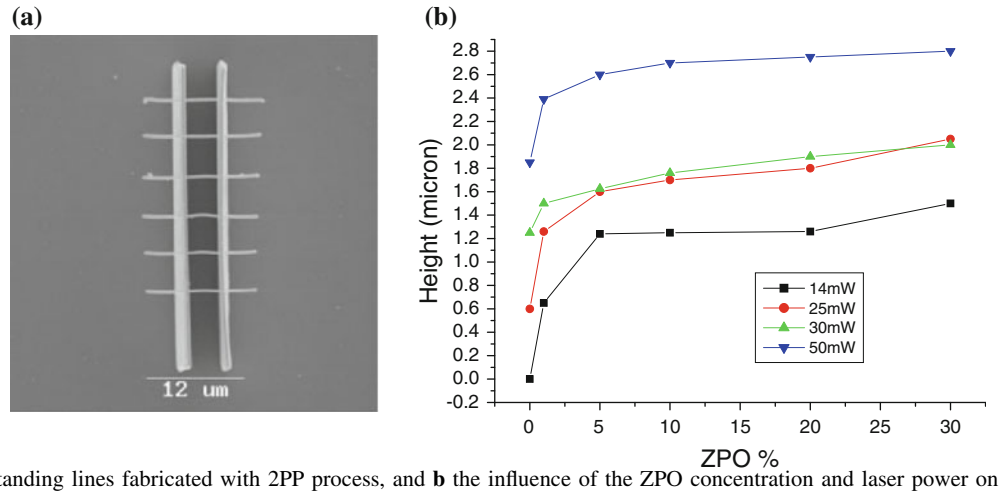

Fig. 11 **a** Free-standing lines fabricated with 2PP process, and **b** the influence of the ZPO concentration and laser power on the voxel height

observed behaviour and can be performed by analysing z-scan measurements at 780 nm, and this will be the subject of a future publication.

Conclusion

Interactions between three commercially available photoinitiators and co-hybrid organo-silicato-zirconate materials have been investigated. UV–Visible spectroscopy was employed to identify the evolution of the photoinitiators absorption as the material composition was adjusted in order to change the properties of the matrix. Unlike the amino-functionalized photoinitiators, the absorption of I-184 is shown to be unchanged by the presence of the matrix either in the liquid or solid phase. However, the spectral absorptions of DB and I-369 have undergone a red shift, indicating the presence of interactions at the molecular level between both these photoinitiators and the material matrix in which they were dispersed. Moreover, DB has shown the appearance of an extra band centred around 470 nm, the contribution of which was strongly affected by either the concentration of the zirconate monomer, the nature of the chelating agent or the degree of chelation of the zirconium atom. These phenomena have been identified to originate from the occurrence of the metal ligand charge transfer process between the zirconium complex and the amino-functionalized photoinitiators, which is significantly affected by the degree of condensation of the material. These materials have been shown to have almost ideal characteristics for microstructuring by conventional UV-lithography and the 2PP technique (high photoreactivity, low shrinkage). In this context, the findings of this study can be used as a basis for the future design of more efficient photoinitiators.

UV-lithography and 2PP processes will benefit from the study presented in this article as it can be used as a basis for the design of more efficient photoinitiators in the future.

Acknowledgements The authors wish to thank CIBA Specialty Chemicals Corporation for having generously provided the Irgacures photoinitiators employed in this study, and gratefully acknowledge the financial support of Enterprise Ireland under the "Commercialisation Fund Technology Development" project Multibiosense (TD/08/309). This study was also supported by the DFG Excellence Cluster 'Rebirth' and SFB Transregio 37, and ERASPOT. Authors would also like to thank the LaserLab initiative.

References

1. Kang S, Tai T-Y, Fang T-H (2010) Curr Appl Phys 10:625
2. Pain L, Tedesco S, Constancias C (2006) C R Phys 7:910–923
3. Arpin A, Mihi A, Johnson H-T, Baca A-J, Rogers J-A, Lewis J-A, Braun P-V (2010) Adv Mater 22:1084
4. Lee K-S, Kim RH, Yang D-Y, Park SH (2008) Prog Polym Sci 33:631
5. Houbertz R (2005) Appl Surf Sci 247:504
6. Wolfe DB, Qin D, Whitesides GM (2008) Method Mol Biol 583:81
7. Okano T, Hasegawa M, Yamato M, Kikuchi A, Ishikawa I, Patent number WO2005103233-A1; EP1748064-A1; JP2006512629-X; US2008118474-A1
8. Stavis SM, Strychalski EA, Gaitan M (2009) Nanotechnology 20:165302
9. Jariwala S, Tan B, Venkatakrishnan K (2009) J Micromech Microeng 19:115023
10. Lei C, Patent number WO2009143414-A1; US2009291214-A1
11. Lin S-E, Yu B-Y, Shuye J-J, Wei W-CJ (2008) J Am Ceram Soc 91(12):3976
12. Versace DL, Oubaha M, Copperwhite R, Croutxé-Barghorn C, MacCraith BD (2008) Thin Solid Films 516:6448
13. WeiX T, Hildebrand G, Schade R, Liefeith K (2009) Eng Life Sci 9(5):384
14. Ovsianikov A, Shizhou X, Farsari M, Vamvakaki M, Fotakis C, Chichkov BN (2009) Opt Express 17(4):2143
15. Ovsianikov A, Viertl J, Chichkov BN, Oubaha M, MacCraith BD, Sakellari I, Giakoumaki A, Gray D, Vamvakaki M, Farsari M, Fotakis C (2008) ACS Nano 2(11):2257
16. Ovsianikov A, Gaidukeviciute A, Chichkov BN, Oubaha M, MacCraith BD, Sakellari I, Giakoumaki A, Gray D, Vamvakaki M, Farsari M and Fotakis C (2008) Laser Chemistry, Article ID 493059, 7 pp
17. Oubaha M, Smaïhi M, Etienne P, Coudray P, Moreau Y (2003) J Non-Cryst Solids 318:305
18. Copperwhite R, Oubaha M, Versace DL, Croutxe-Barghorn C, MacCraith BD (2008) J Non-Cryst Solids 354:3617
19. Sun H-B, Kawata S (2004) Adv Polymer Sci 170:169. doi: 10.1007/b94405
20. Ovsianikov A, Passinger S, Houbertz R, Chichkov BN (2006) In: Phipps CR (ed) Springer series in optical sciences. Springer, Berlin, pp 129–167
21. Craver E, McCrate A, Nielsen M, Swavey S (2010) Inorg Chim Acta 363:453
22. Liu T, Zhou X, Pan Q-J, Xia B-H, Zhang H-X (2009) J Organomet Chem 694:150